Change in the Microstructure of Ferritic Stainless Steel with Surface Roughness and the Number of Thermal Cycles

Myoung Youp SONG

Division of Advanced Materials Engineering, Hydrogen and Fuel Cell Research Center, Engineering Research Institute, Jeonbuk National University, 567 Baekje-daero Deokjin-gu Jeonju, 54896, Republic of Korea

crossref http://dx.doi.org/10.5755/j02.ms.29262

Received 06 June 2021; accepted 10 August 2021

One of the candidates for metallic interconnects of solid oxide fuel cells is ferritic stainless steel, Crofer 22 APU. Ferritic stainless steel Crofer 22 APU specimens with different surface roughness were prepared by grinding with SiC powder papers of various grits and then thermally cycled in air. Variation in the microstructure of the samples having different roughness with thermal cycling was investigated. Polished Crofer 22 APU specimens after three and five thermal cycles had relatively flat oxide layers with thicknesses of about 13.8 and 17.9 μm, respectively. Micrographs of a trench made by milling with FIB (focused ion beam) for a Crofer 22 APU specimen ground with grit 80 SiC powder paper after 8 thermal cycles (total oxygen exposure time of 200 h at 1073 K), captured by ESB (energy selective back-scattering) and SE2 (type II secondary electrons), showed that the surface of the sample was very coarse and its oxide layer was undulated. In the oxide layer, the phase of the sublayer was Cr_2O_3, and that of the top layer was $(Cr, Mn)_3O_4$ spinel. The surface of the sample ground with grit 80 SiC powder paper was very rough after 60 thermal cycles (total oxygen exposure time of 1500 h at 1073 K). The polished Crofer 22 APU is a better applicant to an interconnect of SOFC than those with rougher surfaces.

Keywords: fuel cells, interconnect, ferritic stainless steel, thermal cycling, oxidation, microstructure.

1. INTRODUCTION

A repeating unit of fuel cells is composed of interconnect, anode, electrolyte, and cathode. Interconnect materials of a solid oxide fuel cell (SOFC) have been studied together with the automobile-related materials which investigated mechanical properties [1–3], microstructural characterization [4–9], and acoustical properties [10]. In order for a material to be applied to an interconnect material of SOFC [11–14], the material should have appropriate properties from the perspectives of electronic and ionic conductivities in fuel and oxidizing atmospheres, chemical stability in the fuel-cell environment, strength, and toughness, thermal conductivity, and cost. In addition, thermo-mechanical and chemical harmony with adjoining parts in SOFC is required for the material.

The SOFC operating temperature was decreased from 1173–1273 K to 874–1123 K [15] thanks to recent research results, enabling metallic interconnects [16–21] to be used. Metallic interconnects have many advantages over ceramic interconnects, such as lanthanum chromite ($LaCrO_3$) and doped lanthanum chromite [22]. Nevertheless, oxidation of the metallic interconnects under SOFC operation circumstances increases contact resistance, leading to a decrease in electrical conductivity.

Yang et al. [23] studied heat resistance alloys to examine their applicability to SOFC interconnects. They reported that ferritic stainless steels with appropriately selected compositions are the best candidates for SOFC interconnect materials, and either surface or bulk needs to be adjusted in the case of the chromium-forming alloys.

One of the appropriate interconnect alloys is reportedly ferritic stainless steel, Crofer 22 APU, prepared by bulk adjustment. A bulk adjustment was done to enhance oxidation/corrosion resistance and increase scale conductivity. Forschungszentrum Julich of Germany developed Crofer 22 APU, which was made of ~ 23 wt.% Cr and small quantities of Mn, Ni, Al, Si, La, and Ti.

The way how ferritic stainless steels are oxidized under circumstances where one side of the Crofer 22 APU sample was exposed to air and its other side was exposed to moist hydrogen as the fuel was examined by Yang et al. [24]. The scales grown on the air side under these dual exposure SOFC conditions could be significantly different from scales grown on samples exposed to air on both sides. From XRD analysis, they found that Cr_2O_3 and M_3O_4 (M = Cr, Mn, and/or Fe) spinel were formed on both sides of the sample exposed to air during heating. Iron was rich in the spinel upper layer of the scale on the air side of Crofer 22 APU (~ 23 wt.% Cr) sample after isothermal heating at 1073 K, and the rate of the anomalous oxidation was increased as temperature and the number of thermal cycles increased.

In addition to this research, many studies on Crofer 22 APU have been carried out [25–28]. Yang et al. [25] prepared a $Mn_{1.5}Co_{1.5}O_4$ spinel barrier layer on the Crofer 22 APU. They reported that degradation was decreased because the layer prevented chromium from migrating from chromium-forming alloy interconnects into the cathode and improved good electrical contact. The good thermal stability of the spinel protection layer resulted from a good thermal expansion match between Crofer 22 APU substrate and the $Mn_{1.5}Co_{1.5}O_4$ spinel [25].

Contact between interconnect and cathode is related with surface roughness. The surface roughness of interconnects is thus believed to have great effect on the

* Corresponding author. Tel.: +82-10-3260-2379; fax: +82-63-270-2386.
E-mail address: *songmy@jbnu.ac.kr* (M.Y. Song)

electrical properties of interconnects. In the present work, we ground surfaces of Crofer 22 APU pieces (1 × 1 cm squares, 0.8 mm thickness) with SiC powder papers of different grits and prepared Crofer 22 APU specimens with different roughness. They were then thermally cycled between 1073 K and room temperature in air. Change in the microstructure of these specimens with the number of thermal cycles was investigated.

2. EXPERIMENTAL DETAILS

A Crofer 22 APU plate with a thickness of 0.8 mm was cut into 1 × 1 cm squares and ground with SiC powder papers of different grits. The chemical composition of Crofer 22 APU [29 – 32] is given in Table 1. We prepared samples with different surface roughness by grinding with SiC powder papers of various grits and by polishing.

Table 1. The chemical composition (wt.%) of Crofer 22 APU

C	Cr	Mn	Al	Si	Ni	Ti	V	Co	Others	Fe	Ti	V	Co
0.03	23	0.41	0.12	0.1	0.16	0.05	–	–	0.08 La	~76.08	0.05	–	–

Polished samples were cycled by heating to 1073 K with a rate of 5 K/min, maintaining at 1073 K for 100 h, and cooling to room temperature with a rate of 15 K/min in air. The numbers of thermal cycles for the preparation of samples were three and five, with the 1073 K maintenance periods (oxygen exposure time) being 300 h and 500 h, respectively.

Samples ground with 80 and 240 grit SiC powder papers and a polished sample were cycled by heating to 1073 K with a rate of 10 K/min, maintaining at 1073 K for 25 h, and cooling to room temperature with a rate of 10 K/min in air. The numbers of thermal cycles to prepare the samples were 8, 20, and 60, with the 1073 K maintenance periods (oxygen exposure time) being 200, 500, and 1500 h, respectively.

The surfaces of the prepared samples were investigated by scanning electron microscopy (SEM). In addition, trenches were made by milling with the FIB (focused ion beam), and scale/alloy interfaces were observed by ESB (energy selective back-scattering) and SE2 (type II secondary electrons) for the sample ground with grit 80 SiC powder paper and the polished sample thermally-cycled for 8 and 60 times in the air. Phases were analyzed by EDS (energy dispersive spectroscopy).

3. RESULTS AND DISCUSSION

The SEM micrographs for the cross-sections of polished Crofer 22 APU samples after three thermal cycles (total oxygen exposure time of 300 h at 1073 K) and five thermal cycles (total oxygen exposure time of 500 h at 1073 K), each cycle consisting of heating to 1073 K, maintaining at 1073 K for 100 h, and cooling to room temperature, are shown in Fig. 1. For this observation, the surface of the polished Crofer 22 APU sample after cycling was Ni-coated by electroless plating technique [30] and polished after mounting using epoxy resin and hardener. The samples exhibit the alloy, oxide layer, and Ni-coated layer. The oxide layer is relatively flat and has a quite homogeneous thickness. The sample after three cycles shows a broken oxide layer. It is believed that the oxide layer was broken during preparing the sample for SEM observation. Pores are observed between the alloy and the oxide layer and between the oxide layer and the Ni-coated layer in the sample after five thermal cycles. The samples after three and five thermal cycles have thicknesses of about 13.8 and 17.9 μm, respectively. This shows that, as the number of thermal cycles increased, the thickness of the oxide layer increased.

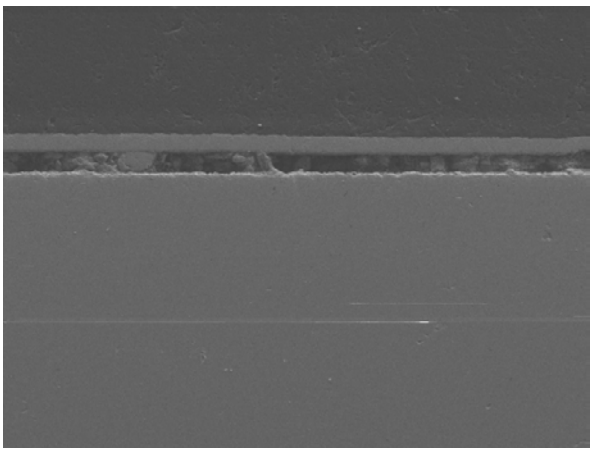

a

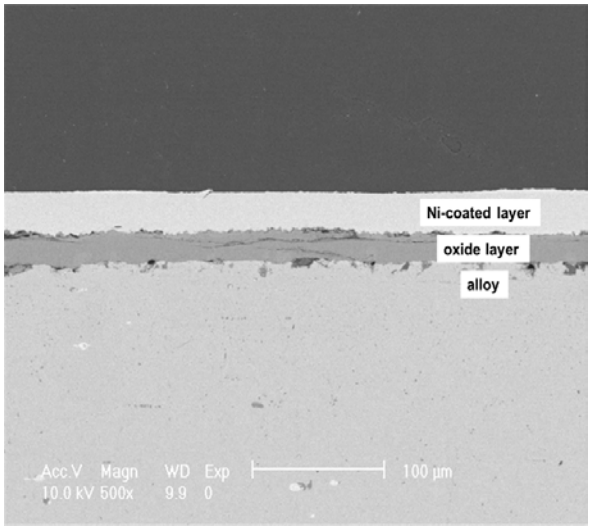

b

Fig. 1. SEM micrographs for the cross-sections of polished Crofer 22 APU samples: a – after three thermal cycles; b – five thermal cycles, each cycle consisting of heating, maintaining at 1073 K for 100 h, and cooling

A micrograph by BSE (back-scattered electron) at high magnification for the cross-section of polished Crofer 22 APU samples after five thermal cycles, each cycle consisting of heating to 1073 K, maintaining at 1073 K for 100 h, and cooling to room temperature, is shown in Fig. 2. Inside the oxide layer, a quite wide crack is observed. We can see grain boundaries inside the alloy. Pores are observed between the oxide layer and the Ni-coated layer.

Fig. 3 shows the SEM micrographs at different magnifications for the surfaces of Crofer 22 APU samples ground with grit 240 SiC powder paper after 8 thermal

cycles, each cycle consisting of heating, maintaining at 1073 K for 25 h, and cooling.

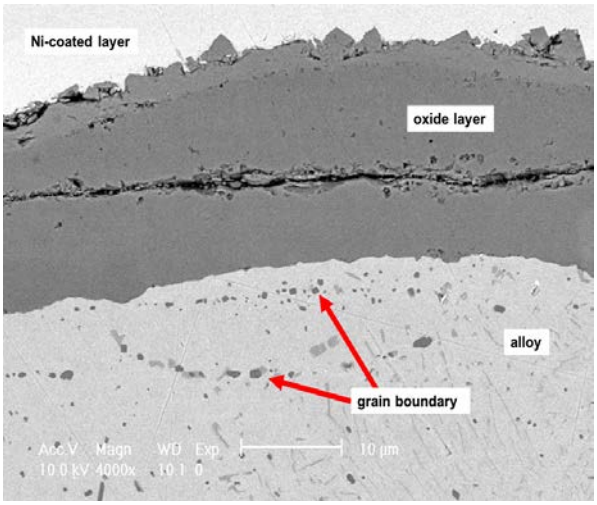

Fig. 2. A micrograph by BSE (back-scattered electron) at high magnification for the cross section of polished Crofer 22 APU samples after five thermal cycles, each cycle consisting of heating, maintaining at 1073 K for 100 h, and cooling

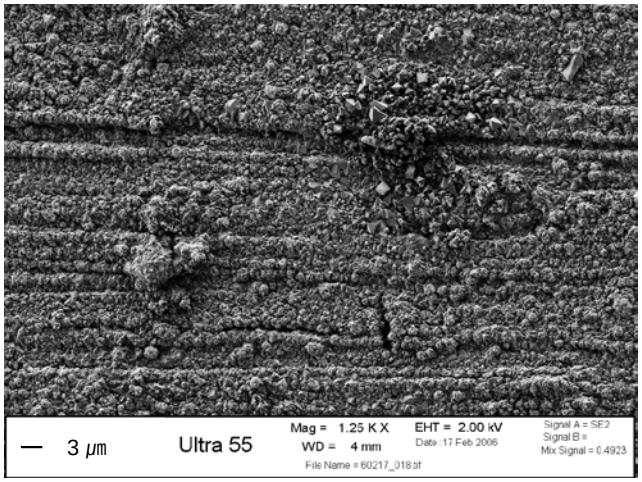

Fig. 3. SEM micrographs at different magnifications for the surfaces of Crofer 22 APU samples ground with grit 240 SiC powder paper after 8 thermal cycles, each cycle consisting of heating, maintaining at 1073 K for 25 h, and cooling

The SEM micrograph at a low magnification exhibits valleys and ridges consisting of particles, and that at high magnification exhibits the particles which are in shapes of polyhedron with flat surfaces of various sizes.

The SEM micrographs at different magnifications for the surfaces of Crofer 22 APU samples ground with grit 240 SiC powder paper after 20 thermal cycles, each cycle consisting of heating, maintaining at 1073 K for 25 h, and cooling, are shown in Fig. 4.

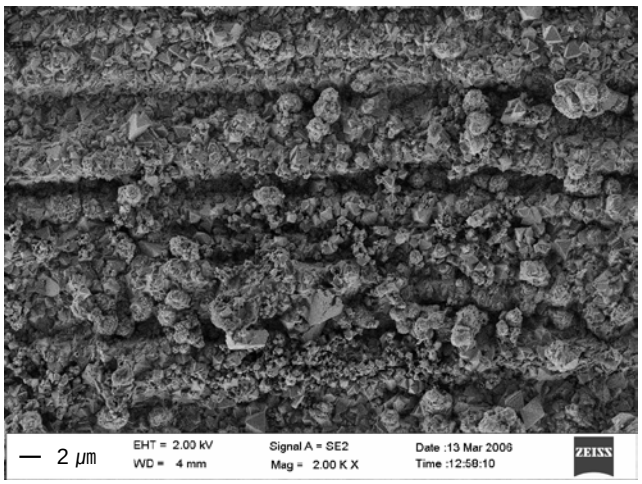

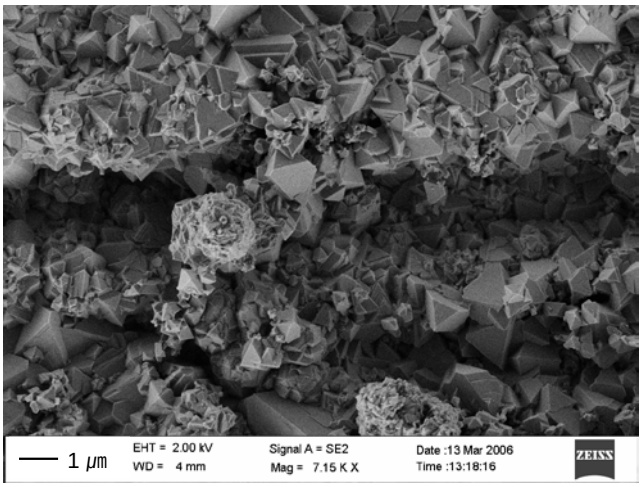

Fig. 4. SEM micrographs at different magnifications for the surfaces of Crofer 22 APU samples ground with grit 240 SiC powder paper after 20 thermal cycles, each cycle consisting of heating, maintaining at 1073 K for 25 h, and cooling

The sample exhibits a microstructure similar to that of the sample after 8 thermal cycles (shown in Fig. 3), having deeper valleys and higher ridges consisting of larger particles than those of the sample after 8 thermal cycles. The particles are in shapes of polyhedron with flat surfaces of larger sizes than those of the sample after 8 thermal cycles (shown in Fig. 3).

Fig. 5 shows a SEM micrograph at high magnification for the surface of the Crofer 22 APU sample ground with grit 240 SiC powder paper after 20 thermal cycles, each cycle consisting of heating, maintaining at 1073 K for 25 h, and cooling. A particle made of polyhedrons with flat surfaces looks like a rose. Large flat surfaces forming particles are also observed.

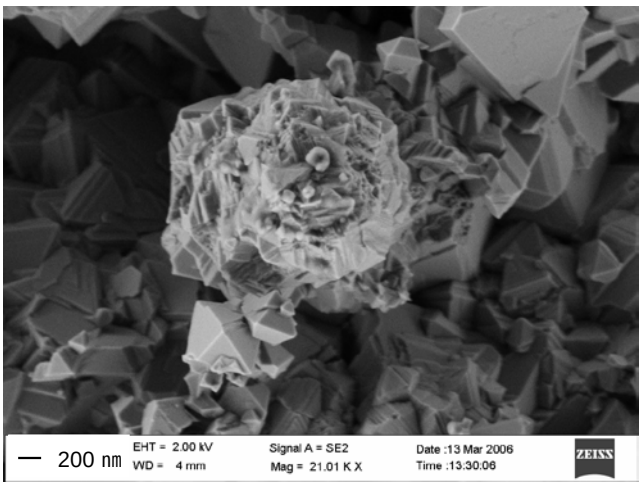

Fig. 5. SEM micrograph at high magnification for the surface of the Crofer 22 APU sample ground with grit 240 SiC powder paper after 20 thermal cycles, each cycle consisting of heating, maintaining at 1073 K for 25 h, and cooling

The micrographs of a trench made by milling with the FIB (focused ion beam) for a Crofer 22 APU sample ground with grit 80 SiC powder paper after 8 thermal cycles, captured by ESB and SE2, are shown in Fig. 6. Each cycle consisted of heating, maintaining at 1073 K for 25 h, and cooling to room temperature. The surface of the sample is very coarse. The oxide layer is undulated with a thickness of about 0.6 μm. The phases are marked. In the oxide layer, the Cr_2O_3 phase develops near the side of the alloy, and the (Cr, Mn)$_3O_4$ spinel phase forms outside the Cr_2O_3 phase. The micrograph captured by ESB shows the boundary between the Cr_2O_3 phase and the (Cr, Mn)$_3O_4$ spinel phase. On the other hand, the micrographs taken by SE do not exhibit the boundary between the Cr_2O_3 phase and the (Cr, Mn)$_3O_4$ spinel phase. The bright region in the oxide layer is believed to appear due to highly concentrated electrons, and the boundary between the Cr_2O_3 and (Cr, Mn)$_3O_4$ phases is believed to be located in the middle of the oxide layer.

Fig. 7 shows the micrographs at different magnifications captured by ESB of a trench made by milling with the FIB for a polished Crofer 22 APU sample after 8 thermal cycles, each cycle consisting of heating, maintaining at 1073 K for 25 h, and cooling. The oxide layer is straighter, compared with that formed in the sample ground with grit 80 SiC powder paper after 8 thermal cycles. The phases are marked. In the oxide layer with a thickness of about 0.8 μm, the Cr_2O_3 phase develops near the side of the alloy, and the (Cr, Mn)$_3O_4$ spinel phase forms outside the Cr_2O_3 phase. Grain boundaries are observed.

The micrographs captured by ESB and SE2 of a trench made by milling with the FIB, for a Crofer 22 APU sample ground with grit 80 SiC powder paper after 60 thermal cycles, are shown in Fig. 8. Each cycle consisted of heating to 1073 K, maintaining at 1073 K for 25 h, and cooling to room temperature. The surface of the sample is very rough. Some ridges are quite straight and continuous. The phases (alloy, Cr_2O_3, and (Cr, Mn)$_3O_4$ spinel) are marked in the micrographs.

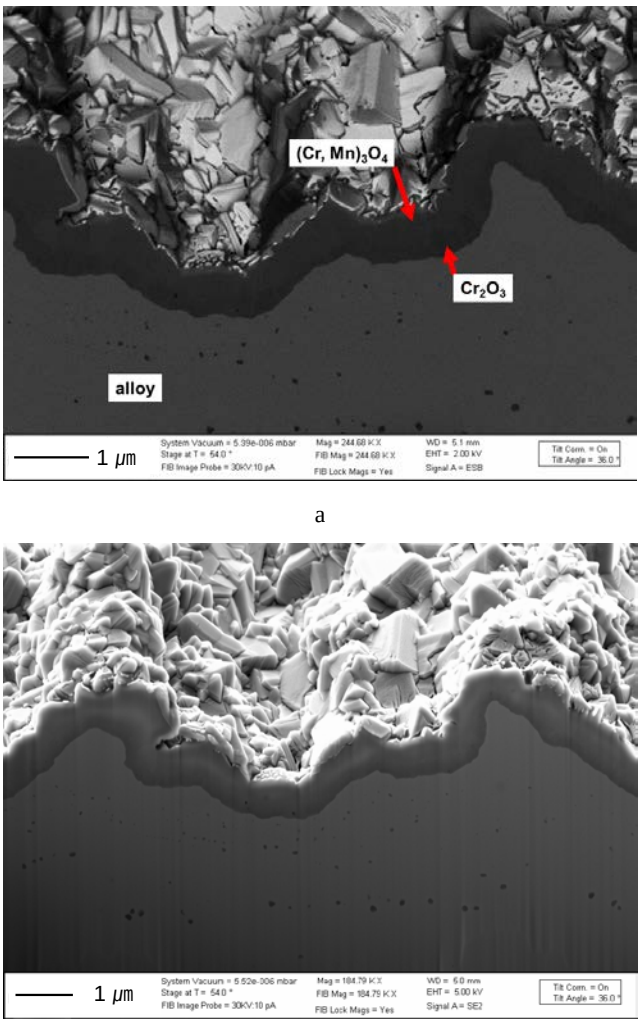

a

b

Fig. 6. Micrographs of a trench made by milling with the FIB (focused ion beam) for a Crofer 22 APU sample ground with grit 80 SiC powder paper after 8 thermal cycles, each cycle consisting of heating, maintaining at 1073 K for 25 h, and cooling, captured by: a – ESB (energy selective back-scattering); b – SE2 (type II secondary electrons)

In the oxide layer with a thickness of about 2.1 μm, the Cr_2O_3 phase develops near the side of the alloy, and the (Cr, Mn)$_3O_4$ spinel phase forms outside the Cr_2O_3 phase. The micrograph captured by ESB shows clearly the boundary between the Cr_2O_3 phase and the (Cr, Mn)$_3O_4$ spinel phase. The (Cr, Mn)$_3O_4$ spinel phase in shapes of a polyhedron with flat surfaces can be observed clearly on the sample surface in Fig. 8 b. The sample ground with grit 80 SiC powder paper after 60 thermal cycles had a thicker oxide layer (about 2.1 μm) than that after 8 thermal cycles (about 0.6 μm). Compared with the oxide layer of the polished sample, the oxide layer of the sample ground with grit 80 SiC powder paper is more undulated.

As the number of thermal cycles increased, the quantities of formed Cr_2O_3 and (Cr, Mn)$_3O_4$ spinel phases increased. The (Mn, Co)$_3O_4$ spinel phase has high electrical conductivity, and the formation of Cr_2O_3 increases the electrical resistance. With an increasing number of thermal cycles, the oxide layer got thicker, leading to an increase in area specific resistance (ASR).

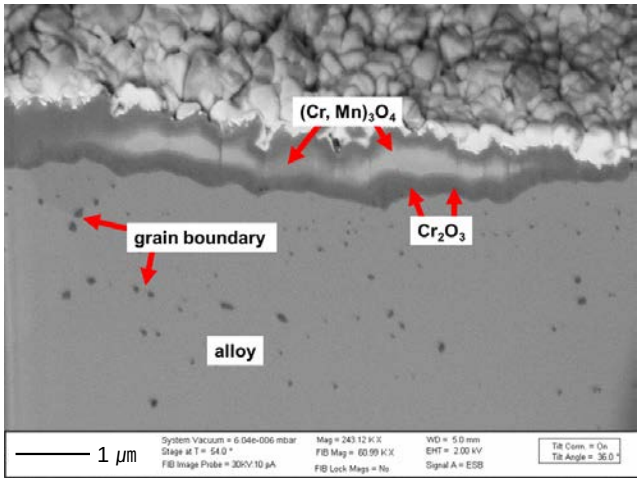

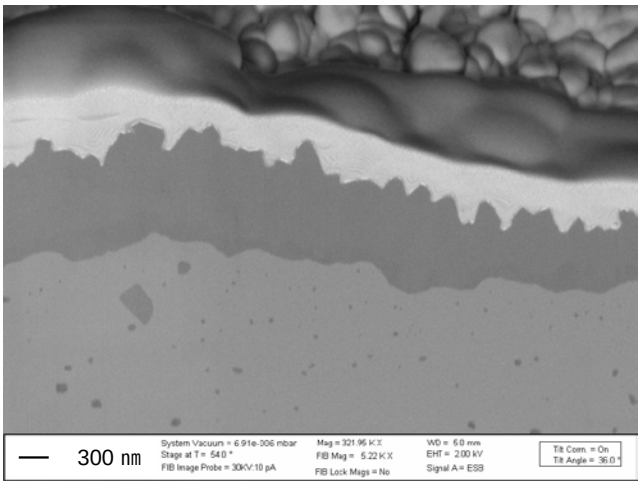

Fig. 7. Micrographs at different magnifications captured by ESB of a trench made by milling with the FIB for a polished Crofer 22 APU sample after 8 thermal cycles, each cycle consisting of heating, maintaining at 1073 K for 25 h, and cooling

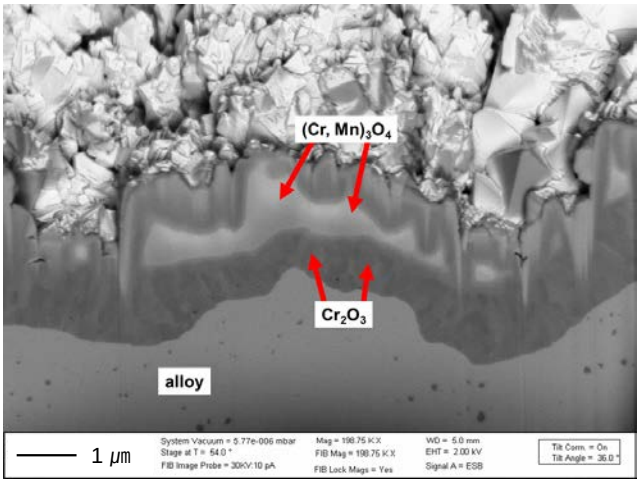

a

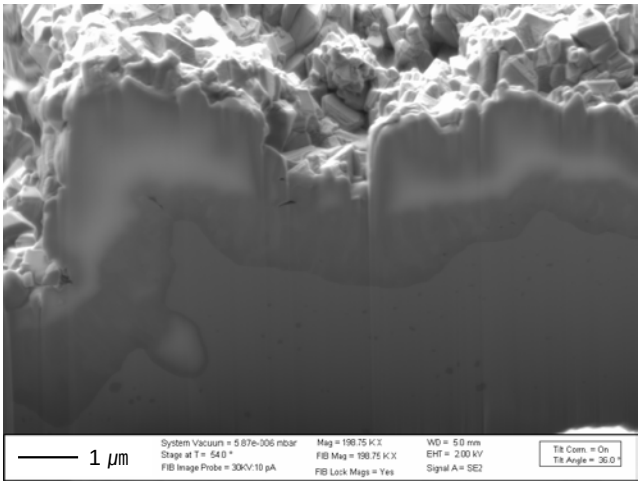

b

Fig. 8. Micrographs captured by: a – ESB; b – SE2 of a trench made by milling with the FIB, for a Crofer 22 APU sample ground with grit 80 SiC powder paper after 60 thermal cycles

As the number of a grit of used emery paper decreased, the oxide layer was more undulated. A more undulated oxide layer has larger electrical resistance because the contact between the cathode and interconnect is poorer than a flat oxide layer. The oxidation rate in an undulated layer is believed to be higher than that in a flat layer because the former has a larger surface area than the latter.

Zhu et al. [33] reported that chromia (Cr_2O_3) produced on the surface of chromium-based alloys are intrinsically too volatile to be applicable as interconnects for SOFCs operating above 1073 K, some intermediate phases occurring between iron-based interconnect and cathode significantly increase the contact resistance, and metallic materials that form stable oxide scales with acceptable growth rate and reasonably high electrical conductivity over the expected SOFC lifetime need to be developed. Zhu et al. [33] investigated oxidation behaviors of two specimens, 304 and 430 stainless steels with and without different pre-surface treatments on the surface. The polished samples have traces of polishing on the surfaces [33]. The as-received samples have smaller grains than the sand-blast samples.

After exposure to the oxidation atmosphere, the as-received samples have the smallest grains, followed in order by the polished samples and the sand-blast samples. The as-received samples also have some large grains. After 100 h exposure to the oxidation atmosphere, the polished, the as-received, and the sand-blast STS430 samples had the formed oxide layer thicknesses of about 4.2, 7.5, 3.1 μm, respectively [33], showing that the sand-blast sample has the highest high-temperature oxidation stability, followed in order by the polished and the as-received samples. The Al_2O_3 on the surface deposited during sand-blasting is believed to reduce the formation rate of Cr_2O_3 at high-temperature oxidation atmosphere [33]. The authors reported that the oxidation progresses along the grain boundaries. Cracks and pores are believed to be formed among the finest grains of the as-received samples. Oxygen then penetrates through them and oxides form. These are thought to have led to the formation of the thickest oxide layer in the as-received samples [33].

Shim [30] reported that technical problems must be solved to apply chromia scale forming ferritic stainless steel in the environment of the SOFC stack. The chromium

scale that develops at the interconnect/contact interface leads to very high electrical resistance and severe degradation of cell performance [30]. Scale growth leads to crack formation and subsequent delamination, the accumulation of pores at the metal/scale interface, cracking and spallation, and wrinkling of the oxide scale [30].

That the inherent volatility of high-valent chromium compounds not only accelerates the oxidation rate but also causes chromium diffusion into the porous cathode was also reported by Shim [30]. Under such conditions, reduction and deposition of chromium compounds such as Cr_2O_3, occurring at the cathode/electrolyte interface, may greatly reduce the electro-catalytic reaction efficacy of triple-phase boundary regions [30].

Shim [30] reported that during the early stage of oxidation, both chromia and spinel phases nucleated on the alloy surface, and coarse spinel phases were formed on the chromia subscale. As oxidation time increased, the top surface of oxide became to be covered with spinel phases. Oxide growth through alloy grain boundaries was pronounced in Crofer 22 APU [30]. The evolution of the scale's microstructure and chemical composition were directly related to ASR. Crofer 22 APU appears to be the most promising alloy for SOFC interconnect applications among tested Fe-Cr based stainless steels (Crofer 22 APU, ZMG232L, and SS430) and a Ni-Cr based alloy (Haynes 230) [30].

Moon et al. [34] reported that the electrical conductivity of a metallic interconnect depends largely on the electrical conductivities of the oxides formed on the surface and pre-surface treatments of metallic interconnects are required to reduce their oxidation rates.

Yang et al. [24] reported that Cr_2O_3 and M_3O_4 (M = Cr, Mn, and/or Fe) spinel were formed on both sides of the sample exposed to air during heating and the rate of the anomalous oxidation was increased as temperature and the number of thermal cycles increased. Yang et al. [25] also reported that a $Mn_{1.5}Co_{1.5}O_4$ spinel barrier layer prepared on the crofer22 APU decreased degradation because the layer prevented chromium from migrating from chromium forming alloy interconnects into the cathode and improved good electrical contact. To minimize scale growth rate and Cr migration to the cathode, perovskite and spinel coatings by pulsed laser deposition, electrical spray deposition, or screen printing were suggested by Shim [30].

ASR was measured for prepared samples. ASR decreased as the number of the grit of used emery paper increased, suggesting that the polished Crofer 22 APU is a better applicant to interconnects of SOFC than those with rougher surfaces.

4. CONCLUSIONS

Variation in the microstructure of the Crofer 22 APU samples having different roughness with thermal cycling was investigated. Polished Crofer 22 APU specimens after three and five thermal cycles had relatively flat oxide layers with thicknesses of about 13.8 and 17.9 μm, respectively. The SEM micrograph for the surfaces of Crofer 22 APU samples ground with grit 240 SiC powder paper after 8 thermal cycles, each cycle consisting of heating, maintaining at 1073 K for 25 h, and cooling to room temperature, clearly exhibited valleys and ridges consisting of particles, and the particles in shapes of a polyhedron with flat surfaces of various sizes. Micrographs of a trench made by milling with the FIB (focused ion beam) for a Crofer 22 APU sample ground with grit 80 SiC powder paper after 8 thermal cycles (total oxygen exposure time of 200 h at 1073 K), captured by ESB and SE2, showed that the surface of the sample was very coarse and its oxide layer was undulated. In the oxide layer, the Cr_2O_3 phase developed near the side of the alloy, and the $(Cr, Mn)_3O_4$ spinel phase formed outside the Cr_2O_3 phase. The sample ground with grit 80 SiC powder paper after 60 thermal cycles had a thicker oxide layer (about 2.1 μm) than that after 8 thermal cycles (about 0.6 μm). Compared with the oxide layer of the sample ground with grit 80 SiC powder paper, the oxide layer of the polished sample was less undulated. The polished Crofer 22 APU is a better applicant to an interconnect of SOFC than those with rougher surfaces.

REFERENCES

1. **Otaru, A.J.** Review on Processing and Fluid Transport in Porous Metals with a Focus on Bottleneck Structures *Metals and Materials International* 26 2020: pp. 510 – 525. https://doi.org/10.1007/s12540-019-00345-9
2. **Zafar, M.Q., Zhao, H.** 4D Printing: Future Insight in Additive Manufacturing *Metals and Materials International* 26 2020: pp. 564 – 585. https://doi.org/10.1007/s12540-019-00441-w
3. **Shin, D.S., Kim, S.H., Oh, J.W., Jung, I.D., Yang, W.S., Lee, C.H., Kwon, H.J., Koo, J.M., Park, S.J.** Correlation Study between Material Parameters and Mechanical Properties of Iron–Carbon Compacts Using Sensitivity Analysis and Regression Model *Metals and Materials International* 25 2019: pp. 1258 – 1271. https://doi.org/10.1007/s12540-019-00278-3
4. **Ananiadis, E., Lentzaris, K., Georgatis, E., Mathiou, C., Poulia, A., Karantzalis, A.E.** AlNiCrFeMn Equiatomic High Entropy Alloy: a Further Insight in Its Microstructural Evolution, Mechanical and Surface Degradation Response *Metals and Materials International* 26 2020: pp. 793 – 811. https://doi.org/10.1007/s12540-019-00401-4
5. **Siow, K.S., Chua, S.T.** Thermal Ageing Studies of Sintered Micron-Silver (Ag) Joint as a Lead-Free Bonding Material *Metals and Materials International* 26 2020: pp. 1404 – 1414. https://doi.org/10.1007/s12540-019-00394-0
6. **Behera, P.K., Misra, S.M., Mondal, K.** Effect of Microstructures on the Corrosion Behavior of Reinforcing Bars (Rebar) Embedded in Concrete *Metals and Materials International* 25 2019: pp. 1209 – 1226. https://doi.org/10.1007/s12540-019-00288-1
7. **Molnárová, O., Dvorský, D., Křivský, L., Vojtěch, D.** Specific Response of Additively Manufactured AlSi9Cu3Fe Alloy to Precipitation Strengthening *Metals and Materials International* 26 2020: pp. 1168 – 1181. https://doi.org/10.1007/s12540-019-00504-y
8. **Rastegari, S., Salahinejad, E.** Morphological Optimization of Chemical-Conversion Sodium Titanate and Chitosan/Glass Nanocomposite Dip Coatings Deposited on a Titanium Alloy *Metals and Materials International* 26 2020: pp. 188 – 195.

https://doi.org/10.1007/s12540-019-00315-1

9. **Shafiee, A., Nili-Ahmadabadi, M., Kim, H.S., Jahazi, M.** Development and Microstructural Characterization of a New Wrought High Entropy Superalloy *Metals and Materials International* 26 2020: pp. 591 – 602. https://doi.org/10.1007/s12540-019-00360-w
10. **Otaru, A.J.** Review on the Acoustical Properties and Characterisation Methods of Sound Absorbing Porous Structures: a Focus on Microcellular Structures Made by a Replication Casting Method *Metals and Materials International* 26 2020: pp. 915 – 932. https://doi.org/10.1007/s12540-019-00512-y
11. **Kang, Y.J., Jung, S.H., An, Y.T., Choi, B.H., Ji, M.J.** Electrical Conductivity of Ni-YSZ Anode for SOFCs According to the Ni Powder Size Variations in Core-Shell Structure *Korean Journal of Metals and Materials* 53 2018: pp. 287 – 293. https://doi.org/ 10.3365/KJMM.2015.53.4.287
12. **Seo, S.W., Jung, S.J., Park, M.W., Yu, S.M., Lee, K.T.** Effects of Strontium Gallate Addition on Sintering Behavior and Electrical Conductivity of Yttria-Doped Ceria *Electronic Materials Letters* 10 2014: pp. 213 – 216. https://doi.org/ 10.1007/s13391-013-3026-1
13. **Seo, S.W., Park, J.H., Park, M.W., Koo, J.H., Lee, K.T., Lee, J.S.** Effects of Gallia Addition on Sintering Behavior and Blectrical Conductivity of Yttria-Doped Ceria *Electronic Materials Letters* 10 2014: pp. 791 – 794. https://doi.org/10.1007/s13391-014-3242-3
14. **Kim, H.K., Lee, S.H., Lee, S.G., Lee, Y.H.** Densification Mechanism of $BaTiO_3$ Films on Cu Substrates Fabricated by Aerosol Deposition *Electronic Materials Letters* 11 2015: pp. 388 – 397. https://doi.org/10.1007/s13391-015-4419-0
15. **Park, C.H., Baik, K.H.** Improvements in Oxidation Resistance and Conductivity of Fe-Cr Metallic Interconnector by $(La_{0.8}Ca_{0.2})(Cr_{0.9}Co_{0.1})O_3$ Coating *Metals and Materials International* 20 2014: pp. 63 – 67. https://doi.org/10.1007/s12540-014-1005-1
16. **Chen, L., Yang, Z., Jha, B., Xia, G., Stevenson, J.W.** Clad Metals, Roll Bonding and Their Applications for SOFC Interconnects *Journal of Power Sources* 152 2005: pp. 40 – 45. https://doi.org/10.1016/j.jpowsour.2005.01.055
17. **Linder, M., Hocker, T., Holzer, L., Pecho, O., Andreas Friedrich, A., Morawietz, T., Hiesgen, R., Kontic, R., Iwnschitz, B., Mai, A., Andreas Schuler, J.** Ohmic Resistance of Nickel Infiltrated Chromium Oxide Scales in Solid Oxide Fuel Cell Metallic Interconnects *Solid State Ionics* 283 2015: pp. 38 – 51. https://doi.org/10.1016/j.ssi.2015.11.003
18. **Magrasó, A., Falk-Windisch, H., Froitzheim, J., Svensson, J.E., Haugsrud, R.** Reduced Long Term Electrical Resistance in Ce/Co-Coated Ferritic Stainless Steel for Solid Oxide Fuel Cell Metallic Interconnects *International Journal of Hydrogen Energy* 40 2015: pp. 8579 – 8585. https://doi.org/10.1016/j.ijhydene.2015.04.147
19. **Lin, C.K., Liu, Y.A., Wu, S.H., Liu, C.K., Lee, R.Y.** Joint Strength of a Solid Oxide Fuel Cell Glass–Ceramic Sealant with Metallic Interconnect in a Reducing Environment *Journal of Power Sources* 280 2015: pp. 272 – 288. https://doi.org/10.1016/j.jpowsour.2015.01.126
20. **Jhang, W., Yan, D., Yang, J., Chen, J., Chi, B., Pu, J., Li, J.** A Novel Low Cr-Containing Fe–Cr–Co Alloy for Metallic Interconnects in Planar Intermediate Temperature Solid Oxide Fuel Cells *Journal of Power Sources* 271 2014: pp. 25 – 31. https://doi.org/10.1016/j.jpowsour.2014.07.170
21. **Wu, W., Guan, W., Wang, G., Liu, W., Zhang, Q., Chen, T., Wnag, W.G.** Evaluation of $Ni_{80}Cr_{20}/(La_{0.75}Sr_{0.25})_{0.95}MnO_3$ Dual Layer Coating on SUS 430 Stainless Steel Used as Metallic Interconnect for Solid Oxide Fuel Cells *International Journal of Hydrogen Energy* 39 2014: pp. 996 – 1004. https://doi.org/10.1016/j.ijhydene.2013.10.094
22. **Minh, N.Q.** Ceramic Fuel Cells *Journal of the American Ceramic Society* 76 1993: pp. 563 – 588. https://doi.org/10.1111/j.1151-2916.1993.tb03645.x
23. **Yang, Z., Scott Weil, K., Paxton, D.M., Stevenson, J.W.** Selection and Evaluation of Heat-Resistant Alloys for SOFC Interconnect Applications *Journal of the Electrochemical Society* 150 2003: pp. A1188 – 1201. https://doi.org/10.1149/1.1595659
24. **Yang, Z., Walker, M.S., Stevenson, J.W., Norby, T.** Oxidation Behavior of Ferritic Stainless Steels under SOFC Interconnect Exposure Conditions *Journal of the Electrochemical Society* 151 2004: pp. B669 – 678. https://doi.org/10.1149/1.1810393
25. **Yang, Z., Xia, G., Stevenson, J.W.** $Mn_{1.5}Co_{1.5}O_4$ Spinel Protection Layers on Ferritic Stainless Steels for SOFC Interconnect Applications *Electrochemical and Solid State Letters* 8 2005: pp. A168 – 170. https://doi.org/10.1149/1.1854122
26. **Yang, Z., Xia, G., Simner, S.P., Stevenson, J.W.** Thermal Growth and Performance of Manganese Cobaltite Spinel Protection Layers on Ferritic Stainless Steel SOFC Interconnects *Journal of The Electrochemical Society* 152 2005: pp. A1896 – 1901. https://doi.org/10.1149/1.1990462
27. **Pyo, S.S., Lee, S.B., Lim, T.H., Song, P.H., Shin, D.R., Hynn, S.H., Yoo, Y.S.** Characteristic of $(La_{0.8}Sr_{0.2})_{0.98}MnO_3$ Coating on Crofer 22 APU Used as Metallic Interconnects for Solid Oxide Fuel Cell *International Journal of Hydrogen Energy* 36 2011: pp. 1868 – 1881. https://doi.org/10.1016/j.ijhydene.2010.01.093
28. **Miguel-Pérez, V., Martínez-Amesti, A., Nó, M.L., Larrañaga, A., Arriortua, M.I.** Oxide Scale Formation on Different Metallic Interconnects for Solid Oxide Fuel Cells *Corrosion Science* 60 2012: pp. 38 – 49. https://doi.org/10.1016/j.corsci.2012.04.014
29. **Konysheva, E., Laatsch, J., Wessel, E., Tietz, F., Christiansen, N., Singheiser, L., Hilpert, K.** Influence of Different Perovskite Interlayers on the Electrical Conductivity between $La_{0.65}Sr_{0.3}MnO_3$ and Fe/Cr-Based Steels *Solid State Ionics* 177 (9 – 10) 2006: pp. 923 – 930. https://doi.org/10.1016/j.ssi.2006.01.046
30. **Shim, S.** Material Engineering for Next Generation Solid Oxide Fuel Cells. Ph D. thesis, University of California Irvine. 2007.
31. **Song, M.Y., Mumm, D.R., Song, J., Yoon, S.D.** Formation of Phases and Variation of Area Specific Resistance with Surface Roughness in Oxidized Crofer 22 APU *Korean Journal of Metals and Materials* 52 2014: pp. 41 – 46. https://doi.org/10.3365/KJMM.2014.52.1.041
32. **Mumm, D.R., Song, M.Y.** Variation of Microstructure and Area Specific Resistance with Surface Roughness of a Ferritic Stainless Steel after Long-Term Oxygen Exposure *Korean Journal of Metals and Materials* 53 2015: pp. 270 – 276. https://doi.org/10.3365/KJMM.2015.53.4.270

33. **Zhu, W.Z., Deevi, S.C.** Development of Interconnect Materials for Solid Oxide Fuel Cells *Materials Science and Engineering* A348 2003: pp. 227 – 243. https://doi.org/10.1016/S0921-5093(02)00736-0

34. **Moon, M.S., Woo, K.D., Kim, S.H., Yo, M.H.** Effect of Surface Treatments of Stainless Steels on Oxidation Behavior under Operating Condition of IT SOFC Interconnect *Korean Journal of Metals and Materials* 49 2014: pp. 25 – 31. https://doi.org/10.3365/KJMM.2011.49.1.025